

Minimal and nonminimal universal extra dimension models in the light of LHC data at 13 TeV

Avnish,^{1,2,*} Kirtiman Ghosh,^{1,2,†} Tapoja Jha,^{1,2,‡} and Saurabh Niyogi^{3,§}

¹*Institute of Physics, Sachivalaya Marg, Bhubaneswar, Odisha 751005, India*

²*Homi Bhabha National Institute, Training School Complex, Anushakti Nagar, Mumbai 400085, India*

³*Gokhale Memorial Girls' College, University of Calcutta,
1/1 Harish Mukherjee Road, Kolkata 700 020, India*



(Received 6 March 2021; accepted 10 May 2021; published 9 June 2021)

Universal extra dimension (UED) is a well-motivated and well-studied scenario. One of the main motivations is the presence of a dark matter (DM) candidate, namely the lightest level-one Kaluza-Klein particle, in the particle spectrum of UED. The minimal version of UED (mUED) scenario is highly predictive with only two parameters, namely the radius of compactification and cutoff scale, to determine the phenomenology. Therefore, stringent constraint results from the WMAP/PLANCK measurement of DM relic density (RD) of the Universe. The production and decays of level-one quarks and gluons in UED scenarios give rise to multijet final states at the Large Hadron Collider (LHC) experiment. We study the ATLAS search for multijet plus missing transverse energy signatures at the LHC with 13 TeV center-of-mass energy and 139 inverse femtobarn integrated luminosity. In view of the fact that the DM RD allowed part of mUED parameter space has already been ruled out by the ATLAS multijet search, we move on to a less restricted version of UED, namely the nonminimal UED (nmUED), with nonvanishing boundary-localized terms (BLTs). The presence of BLTs significantly alters the dark matter as well as the collider phenomenology of nmUED. We obtain stringent bounds on the BLT parameters from the ATLAS multijet plus missing transverse energy search.

DOI: [10.1103/PhysRevD.103.115011](https://doi.org/10.1103/PhysRevD.103.115011)

I. INTRODUCTION

After almost a decade long running, the Large Hadron Collider (LHC) collected and analyzed 139 fb^{-1} integrated luminosity data along with a boasting discovery of the Higgs boson [1,2], confirming the mechanism behind masses of the weak gauge bosons and fermions of the Standard Model (SM). Numerous analyses of the LHC data in a variety of channels establish the predictions of the SM on firm footing [2]. Nonetheless, the existence of the Higgs boson brings forth other questions in terms of the stability of its mass, etc. On the experimental front, the evidence of neutrino oscillation, and hence the presence of tiny neutrino masses, casts a shadow over the SM. One can, in principle, solve this problem by incorporating right-handed gauge singlet neutrinos and assigning additional Yukawa terms in

the SM, provided the mass hierarchy in the SM fermion sector is acceptable. A rather more daunting task is to incorporate the idea of a new weakly interacting massive particle in the theory in order to explain certain pressing cosmological as well as astronomical evidences in the name of dark matter (DM). Such inadequacies of the SM lead to plenty of novel theories that would come down to the SM at an appropriate limit.

The invocation of theories with extra spatial dimension(s) is of interest for a number of reasons. The most profound ones are the stability of the Higgs boson mass and the related hierarchy problems that were successfully explained by the Arkani-Hamed–Dimopoulos–Dvali model [3,4] and later by the Randall-Sundrum [5,6] model. Extra-dimensional theories can also achieve a light neutrino without introducing any heavy mass scale [7], the unification of gauge couplings [8], and can also account for hierarchies present in the SM fermion masses [9]. Among a variety of extra-dimensional frameworks, we confine ourselves to a particular variant, called the universal extra dimension (UED) model(s), where all the SM fields are allowed to propagate into the space(s) beyond the usual $3 + 1$ -dimensional space-time [10–12]. Of course, there are other prospects of working with such frameworks, such as electroweak symmetry breaking without invoking a fundamental scalar [13], a cosmologically

* avnish@iopb.res.in

† kirti.gh@gmail.com

‡ tapoja.phy@gmail.com

§ saurabhphys@gmail.com

Published by the American Physical Society under the terms of the Creative Commons Attribution 4.0 International license. Further distribution of this work must maintain attribution to the author(s) and the published article's title, journal citation, and DOI. Funded by SCOAP³.

viable dark matter candidate [14,15], a unification scale at a few TeV [16], an explanation for the long lifetime of proton [17], and the number of fermion generations to be an integral multiple of three [18], and above all, a chance to probe the model at collider experiments with its promising signatures [11,19–48].

In this work, we study the collider phenomenology of a couple of simple variants of UED scenarios that are characterized by a single flat universal (accessible to all the SM particles) extra dimension (y), compactified on a S_1/Z_2 orbifold with radius R (oneUED scenarios). In particular, we consider both the *minimal* (mUED) and *nonminimal* (nmUED) versions of the oneUED model. The particle spectrum of oneUED contains infinite towers of Kaluza-Klein (KK) modes (identified by an integer n , called the KK number) for each of the SM fields. The zero modes are identified as the corresponding SM particles. From a four-dimensional perspective, the conservation of the momentum along the fifth direction implies conservation of the KK number. However, the additional Z_2 symmetry ($y \leftrightarrow -y$), which is required to obtain the chiral structure of the SM fermions, breaks the translational invariance along the fifth dimension. As a result, KK-number conservation breaks down at the loop level, leaving behind only a conserved KK parity, defined as $(-1)^n$, which is an automatic outcome of the S_1/Z_2 orbifolding and has several interesting consequences. For example, KK parity ensures the stability of the lightest KK particle (LKP), allows only the pair productions of level-one KK particles at the collider, and prohibits KK modes from affecting electroweak (EW) precision observables at tree level.

OneUED, being a higher-dimensional theory, is non-renormalizable and hence should be treated as an effective theory valid up to a cutoff scale Λ . Apart from the usual, the SM kinetic, Yukawa, and scalar potential terms for the 5D fields, the oneUED Lagrangian also includes additional SM gauge and Lorentz invariant terms like the vectorlike bulk mass terms [38,40,49–51] for the 5D fermions. Furthermore, one can, in principle, also add kinetic (and Yukawa) terms¹ for all the 5D fields at the orbifold-fixed points, i.e., the boundaries of the bulk and the brane [52,53]. The parameters associated with the boundary-localized terms (BLTs) are not *a priori* known quantities (since they are related to ultraviolet completion for such scenarios) and thus would serve as extra free parameters of the theory. In the minimal version of oneUED [54], all BLTs are assumed to vanish at the cutoff scale (Λ) and are radiatively generated at the low scale, which ultimately appears as corrections to the masses of the KK particles.

¹These terms are known as BLTs. It is important to note that the BLTs are only consistent with 4D Lorentz symmetry as well as the gauge symmetry.

Therefore, in addition to the SM parameters, the phenomenology of mUED is determined by only two additional parameters, namely the radius of compactification R and the cutoff scale Λ . Hence, its predictions are very specific and easily testable at different high energy physics (HEP) experiments. As a result, verdicts from different noncollider and collider experiments, like the LHC and various DM experiments, can easily rule out mUED. It has already been shown in the literature [55–57] that the parts of the R^{-1} - Λ plane of mUED that are consistent with the WMAP/PLANCK [58,59] observed relic density (RD) data, are on the verge of being excluded from the direct searches for the KK particles at the LHC. This motivates us to move on to a less restricted version of oneUED with more parameters, namely the BLT parameters. This is where the nonminimal UED comes into the picture. In nmUED, BLT parameters give rise to modifications in the KK particle masses as well as interactions [60–65]. The effect of such alterations is rather dramatic at the colliders as well as at the dark matter experiments. Studies on various phenomenological aspects of nmUED including the LHC phenomenology are abundant in number. In particular, results from the Higgs boson data [66–68] and different DM experiments [69,70] directly constrain the model. Allowed parameter space in accordance with constraints of flavor physics are also obtained [71–74]. Apart from these, a number of theoretical constraints are also placed from unitarity bounds [75], $Z \rightarrow bb$ decay width [76,77], flavor physics [78,79], collider phenomenology [80], and others [81–83] as well.

In this article, we have studied the collider signatures of mUED and nmUED in the context of recent LHC searches for beyond the SM (BSM) scenarios. The level-one KK particles are expected to be in the mass range of a few hundreds of GeV to a few TeVs. Being strongly interacting, the level-one KK quarks (both the singlet $q^{(1)}$ and doublet $Q^{(1)}$) and gluons $G^{(1)}$ can be copiously produced in pairs at the LHC. These, subsequently, decay into the SM particles and the LKP via cascades involving other level-one KK particles. Therefore, the pair productions of the level-one KK particles give rise to generic multijet + multilepton + missing transverse energy² (\cancel{E}_T) signatures at the LHC.

Now turning on to the actual ambit of our work, it is worth mentioning that the LHC collaborations have so far performed dedicated analysis in the multijet as well as multilepton channels in the context of supersymmetric and other BSM scenarios. In particular, the ATLAS Collaboration has studied the signatures of gluino and/or squark (supersymmetric partner of gluon and quark, respectively) pair productions in multijet plus missing transverse energy channels at the LHC at 13 TeV center-

²The LKP, being stable and weakly interacting, escapes the LHC detectors and thus contributes to the missing energy signature.

of-mass energy with 139 fb^{-1} integrated luminosity. Nonobservation of expected signal (over background) results in strong constraints on many sparticle (super-symmetric particle) masses. One can always perform the ditto analysis as done by the ATLAS for any model to constrain the parameter space of that particular model from the LHC data. In this article, we follow this well trodden path and revisit the status of the mUED and nmUED scenarios after the LHC run-II data.

The paper is organized as follows. In the following Sec. II, we describe the ATLAS multijet analysis strategy and validate our methodology by reproducing the ATLAS results. Next, we first look for the status of the minimal version of universal extra dimension under the lens of LHC data collected at 13 TeV. In Sec. IV, we describe the nonminimal UED model. Section IV A comprises the LHC phenomenology of the nmUED model, followed by the concluding remarks in Sec. V.

II. COLLIDER PHENOMENOLOGY

We have closely followed the latest ATLAS $n_j + \cancel{E}_T$ [84] search with 139 fb^{-1} integrated luminosity data at the 13 TeV LHC. Although the analysis in Ref. [84] is dedicated to the search of squarks and gluinos in the context of supersymmetry, the model independent 95% C.L. upper limits on the visible $n_j + \cancel{E}_T$ cross sections ($\langle \epsilon\sigma \rangle_{\text{obs}}^{95}$) for different signal regions (SRs) can be used to constrain the parameter space of other BSM scenarios that also give similar final states. A brief description about the reconstruction of various objects (jets, leptons, etc.), event selection criteria, and definition of different SRs are presented in the following.

Object reconstruction: Jet candidates have been reconstructed using anti- k_T [85] algorithm implemented in FASTJET [86] with jet radius parameter 0.4. Reconstructed jets with $p_T^j > 20 \text{ GeV}$ and $|\eta^j| < 2.8$ are considered for further analysis. Electron (muon) candidates are required to have $p_T^l > 7(6) \text{ GeV}$ and within $|\eta^l| < 2.47(2.7)$. Next, the overlapping between identified leptons and jets in the final state are resolved by discarding any electron/muon candidate lying within a distance $\Delta R < \min(0.4, 0.04 + \frac{10 \text{ GeV}}{p_T^{\sigma/\mu}})$ of any reconstructed jet candidate. Missing transverse momentum vector p_T^{mis} (with magnitude \cancel{E}_T) is reconstructed using all remaining visible entities, viz. jets, leptons, photons, and all calorimeter clusters not associated with such objects. For a signal having n_j jets, effective mass m_{eff} is defined as the scalar sum of \cancel{E}_T and the transverse momenta of all the n_j jet candidates having $p_T > 50 \text{ GeV}$, whereas H_T is calculated as the scalar sum of transverse momentum of all jets with $p_T > 50 \text{ GeV}$ and $|\eta| < 2.8$. After reconstructing different physics objects, events are preselected for further analysis. As supersymmetry (SUSY) and other BSM scenarios are expected to reside in the high mass scale region, events are preselected accordingly, and thus, in

the process, unnecessary events are rejected. The preselection criteria are summarized below.

Preselection criteria: Events containing a leading jet with $p_T^{j_1} > 200 \text{ GeV}$ and at least a second jet with $p_T^{j_2} > 50 \text{ GeV}$ are considered for further analysis. Only zero lepton events are considered, i.e., events with an isolated electron (muon) with $p_T > 7(6) \text{ GeV}$ are vetoed. Events are required to have sufficiently large missing transverse energy ($\cancel{E}_T > 300 \text{ GeV}$) and effective mass ($m_{\text{eff}} > 800 \text{ GeV}$) in order to be considered for further analysis. Events failing to satisfy $\Delta\phi(j_{1,2}, p_T^{\text{mis}})_{\text{min}} > 0.4^3$ are also rejected.

Event selection and signal regions: To make the search process exhaustive, the ATLAS Collaboration [84] has defined various SRs. Each signal region is designed to study a particular region of parameter space, and hence the signal regions are made mutually exclusive as much as possible. The number of jets sets a powerful criterion in achieving this. For instance, in the context of supersymmetry, a pair of gluinos typically gives more jets than squarks in their usual decay modes. Thus, binning different numbers for jets is the first step for segmenting SRs. Moreover, mass splitting of the parent and daughter determines the kinematics of the events. Thus, in addition, specific cuts on different kinematic variables (dubbed as multibin search) have also been applied to target specific mass hierarchies among different BSM particles. In Ref. [84], ATLAS Collaboration has defined ten signal regions for their model independent study of multijet plus missing energy signatures at the LHC running at 13 TeV center-of-mass energy with 139 fb^{-1} integrated luminosity. The signal regions are defined by varying numbers of jet multiplicities (between 2 and 6) along with the minimum value of the effective mass m_{eff} . In view of the high level of agreement between predicted background and observed yield in all signal regions, a model independent 95% C.L. upper limit is set on the visible BSM contribution to the multijet cross section ($\langle \epsilon\sigma \rangle_{\text{obs}}^{95}$) for each signal region. In our analysis, we have used the ATLAS derived bounds on $\langle \epsilon\sigma \rangle_{\text{obs}}^{95}$ in each signal region to constrain the parameter space of mUED and nmUED. For the sake of completeness, we have summarized the definitions of a few relevant signal regions in Table I.⁴

A. Validation

Since we are following the ATLAS multijet analysis, validation of our analysis against the ATLAS results is crucial. In Table 17 of Ref. [84], ATLAS Collaboration has presented a cut-flow table for their simulated gluino pair production events at $\sqrt{s} = 13 \text{ TeV}$ for gluino mass

³ $\Delta\phi(j_i, p_T^{\text{mis}})_{\text{min}}$ is the azimuthal angle between the i th jet and missing transverse momentum vector p_T^{mis} . Jets are ordered according to their p_T hardness ($p_T^{j_1} > p_T^{j_2} > \dots$).

⁴For more details, we refer the reader to Tables 8, 9, and 12 of Ref. [84].

TABLE I. Selection criteria that have been used to define model independent search regions with jet multiplicities two and four are shown. The aplanarity variable is defined as $A = \frac{3}{2}\lambda_3$, where λ_3 is the smallest eigenvalue of the normalized momentum tensor of the jets (see Ref. [87] for details). The model independent 95% C.L. upper limits derived by the ATLAS [84] on the visible BSM contributions to the multijet cross sections ($\langle\epsilon\sigma\rangle_{\text{obs}}^{95}$) for the above signal regions are also provided. The predictions for mUED and nmUED scenarios for three selected benchmark points (BPs), listed in Tables III and IV, respectively, are also presented.

	SR2j-1.6	SR2j-2.2	SR2j-2.8	SR4j-1.0	SR4j-2.2
n_j	≥ 2	≥ 2	≥ 2	≥ 4	≥ 4
$p_T(j_1)$ (GeV)	> 250	> 600	> 250	> 200	> 200
$p_T(j_{i=2,\dots,n_{\text{min}}})$ (GeV)	> 250	> 50	> 250	> 100	> 100
$ \eta(j_{1,\dots,n_{\text{min}}}) $	< 2.0	< 2.8	< 1.2	< 2.0	< 2.0
$\Delta\phi(j_{1,2,(3)}, p_T^{\text{mis}})_{\text{min}}$	> 0.8	> 0.4	> 0.8	> 0.4	> 0.4
$\Delta\phi(j_{i>3}, p_T^{\text{mis}})_{\text{min}}$	> 0.4	> 0.2	> 0.4	> 0.4	> 0.4
Aplanarity	> 0.04	> 0.04
$\frac{\cancel{E}_T}{\sqrt{H_T}} (\sqrt{\text{GeV}})$	> 16	> 16	> 16	> 16	> 16
m_{eff} (TeV)	> 1.6	> 2.2	> 2.8	> 1.0	> 2.2
$\langle\epsilon\sigma\rangle_{\text{obs}}^{95}$ (fb)	1.46	0.78	0.13	0.54	0.14
	mUED predictions (fb)				
BP ₁ ^m	0.35	0.92	0.03	0.28	0.03
BP ₂ ^m	0.96	0.29	0.05	0.58	0.11
BP ₃ ^m	5.25	2.96	0.33	6.41	0.75
	nmUED predictions (fb)				
BP ₁ ^{nm}	1.67	0.61	0.08	0.05	0.03
BP ₂ ^{nm}	0.45	0.93	0.03	0.02	0.01
BP ₃ ^{nm}	0.50	0.32	0.03	0.60	0.08

$m_{\tilde{g}} = 2200$ GeV and the lightest neutralino (the spin-half supersymmetric partners of the SM EW bosons) mass $m_{\tilde{\chi}_1^0} = 600$ GeV. For validation purposes, we have also generated gluino pairs up to two extra partons in MG5_AMC@NLO [88] with the NNPDF23LO [89] parton distribution functions. Subsequent decays, showering, and hadronization are simulated in PYTHIA8.2 [90,91]. The Catani-Krauss-Kuhn-Webber (CKKW-L) merging scheme [92] is employed for matching and merging. Hadronized events are passed into DELPHES3 [93] for object reconstructions and the implementation of cuts. The cut efficiencies supplied by ATLAS are presented alongside ours in Table II. The numbers from our simulation are close with the numbers from the ATLAS analysis. We must mention that similar exercises have been performed for other signal regions as well and the numbers are consistent. However, we do not intend to present them here, but move on to the actual goal of our study.

III. mUED AFTER LHC RUN-II DATA

In this section, the mUED model is put to test under the lens of LHC data collected at 13 TeV. As mentioned in the Introduction, mUED has one extra spatial dimension (y) compactified on a circle of radius R , which signifies the length scale under probe at the LHC. At the tree level, the

masses of KK states for a given KK level are almost degenerate, leaving little space for the decay products to get registered at the LHC detector. In mUED, radiative corrections to the masses play a very crucial role to remove the

TABLE II. Cut-flow table for signal region SR4j-1.0. The cut efficiencies in the second column are provided by the ATLAS Collaboration in Ref. [84]. Cut efficiencies resulting from our simulation are presented in the third column for comparison.

Process	SUSY gluino pair production	
	$m_{\tilde{g}} = 2200$ GeV and $m_{\tilde{\chi}_1^0} = 600$ GeV	
	Absolute efficiency in %	
Cuts	Appendix B of Ref. [84]	Our simulation
Preselection + $n_j \geq 2$	100.0	99.9
$n_j \geq 4$	92.9	93.7
$\Delta\phi(j_{1,2,(3)}, p_T^{\text{mis}})_{\text{min}} > 0.4$	77.6	74.7
$\Delta\phi(j_{i>3}, p_T^{\text{mis}})_{\text{min}} > 0.2$	69.1	64.0
$p_T(j_4) > 100$ (GeV)	61.3	55.7
$ \eta(j_{1,\dots,4}) < 2.0$	55.7	50.2
Aplanarity > 0.04	38.7	33.5
$\frac{\cancel{E}_T}{\sqrt{H_T}} > 16 (\sqrt{\text{GeV}})$	24.1	17.9
$m_{\text{eff}} > 1000$ (GeV)	24.1	17.9

TABLE III. mUED benchmark points and mass spectra of relevant level-one KK particles.

BPs	R^{-1} (TeV)	ΛR	$m_{G^{(1)}}$ (TeV)	$m_{Q^{(1)}}$ (TeV)	$m_{q^{(1)}}$ (TeV)	$m_{W^{(1)}/Z^{(1)}}$ (TeV)	$m_{L^{(1)}}$ (TeV)	$m_{B^{(1)}}$ (TeV)
BP ₁ ^m	2.0	3	2.222	2.143	2.124	2.045	2.022	1.998
BP ₂ ^m	1.75	40	2.341	2.171	2.122	1.877	1.814	1.748
BP ₃ ^m	1.4	30	1.840	1.668	1.710	1.495	1.448	1.399

degeneracy. Loop corrections to the KK masses in an orbifolded theory are logarithmically divergent. Since, mUED is an effective theory that remains valid up to certain cutoff scale (Λ), the radiative corrections are proportional to the logarithm of Λ [54,94,95]. Therefore, the phenomenology of mUED is completely specified by only two parameters: the compactification radius⁵ (R) and the cutoff scale⁶ (Λ). Low energy observables like muon $g-2$ [97,98], flavor changing neutral currents [99–101], $Z \rightarrow b\bar{b}$ decay [102], the ρ parameter [103], $\bar{B} \rightarrow X_s \gamma$ [104], and other electroweak precision tests [105–108] put a lower bound of about 300–600 GeV⁷ on R^{-1} . On the other hand, consistency with WMAP/PLANCK measured [58,59] DM relic density data puts an upper bound of about 1.4 TeV [95] on R^{-1} . Given this upper limit, it is extremely plausible that experiments at the LHC can either discover or rule out mUED, which will be the key focus of discussion in the following.

In order to discuss the production, decay, and the resulting collider signatures of the KK particles and to present the numerical results, we have chosen three benchmark points listed in Table III along with the masses of relevant level-one KK particles. Being strongly interacting, the level-one KK gluons $G^{(1)}$ and singlet ($q^{(1)}$) as well as doublet ($Q^{(1)}$) KK quarks are expected to be copiously pair produced at the LHC at 13 TeV center-of-mass energy. These level-one KK particles subsequently decay to the SM particles and the LKP via on/off shell lighter intermediate KK particles. It is important to mention that in the

framework of the mUED scenario, the mass hierarchies among different level-one KK particles are determined by the radiative corrections only and hence are independent of R^{-1} and Λ . As a result, the decay branching ratios of the level-one KK particles are also practically independent of R^{-1} and Λ . As the spectra in Table III suggest, $G^{(1)}$, being the heaviest among the level-one KK particles, can decay to both singlet ($q^{(1)}$) and doublet ($Q^{(1)}$) quarks with almost⁸ the same branching ratios. A singlet level-one KK quark ($q^{(1)}$) decays only to $B^{(1)}$ in association with a SM quark. Similarly, a doublet level-one KK quark ($Q^{(1)}$) decays preferably to $W^{(1)\pm}$ or $Z^{(1)}$ accompanied by a SM quark. Mass spectra in Table III show that the hadronic decays of the $W^{(1)\pm}$ are closed kinematically. Therefore, it decays to all three level-one KK doublet lepton flavors universally (both $L^{(1)\pm}\nu$ and $L^{(0)\pm}\nu^{(1)}$). Similarly, $Z^{(1)}$ can decay only to $L^{(1)\pm}\nu$ or $\nu^{(1)}\nu$ (with branching fractions being determined by the corresponding SM couplings). The level-one KK leptons finally decay to $B^{(1)}$ and an ordinary (SM) lepton. In all three BPs (in mUED in general), $B^{(1)}$ is the lightest KK particle, i.e., the LKP. Therefore, the production and subsequent decays of level-one KK quarks/gluons at the LHC give rise to a final state consisting of a number of jets and/or leptons and missing transverse momentum. However, the small mass splittings between level-one KK W^\pm/Z and leptons as well as level-one KK leptons and the LKP (see Table III) would render very soft leptons in the final state. Thus, we concentrate only on the hadronic final states to probe the parameter space of mUED at the LHC at $\sqrt{s} = 13$ TeV and 139 fb^{-1} integrated luminosity data as per the ATLAS strategy [84]. Pair productions of level-one KK quarks/gluons are simulated in the MG5_AMC@NLO [88] event generator. The subsequent decays, initial state radiation (ISR), final state radiation (FSR), hadronization, etc. are simulated in PYTHIA8.2. For the purpose of reconstruction and analysis of the events, we designed our own analysis code with very close proximity to the ATLAS utilized object reconstruction criteria and selection cuts.

The results are summarized in Table I and Fig. 1. We present the final exclusion bound in Fig. 1 on the mUED parameter space for each of the SRs listed in Table I. The region in the R^{-1} - ΛR plane to the left of a given exclusion

⁵The inverse of radius of compactification (R^{-1}) determines the overall mass scale of KK particles for a given KK level and hence determines the production cross sections of KK particles at the LHC.

⁶The cutoff scale (Λ) controls the mass splitting between different KK particles for a given KK level and hence determines the kinematics of mUED signatures at the colliders. The perturbativity of the $U(1)$ gauge coupling requires that $\Lambda < 40R^{-1}$. It has been argued in Ref. [96] that a much stronger bound arises from the running of the Higgs boson self-coupling and the stability of the electroweak vacuum. However, the results of Ref. [96] rely on the lowest-order calculations and the inclusion of higher loops can substantially change these results. Therefore, in our analysis, we varied Λ in the range $3\text{--}40R^{-1}$.

⁷KK parity ensures that one-loop mUED corrections to all electroweak observables are cutoff independent [109,110], and thus the low energy constraints on R^{-1} are almost independent of Λ . The observables start showing cutoff sensitivity of various degrees as one goes beyond one loop or considers more than one extra dimension.

⁸There is a slight kinematic preference for $G^{(1)} \rightarrow qq^{(1)}$ decay.

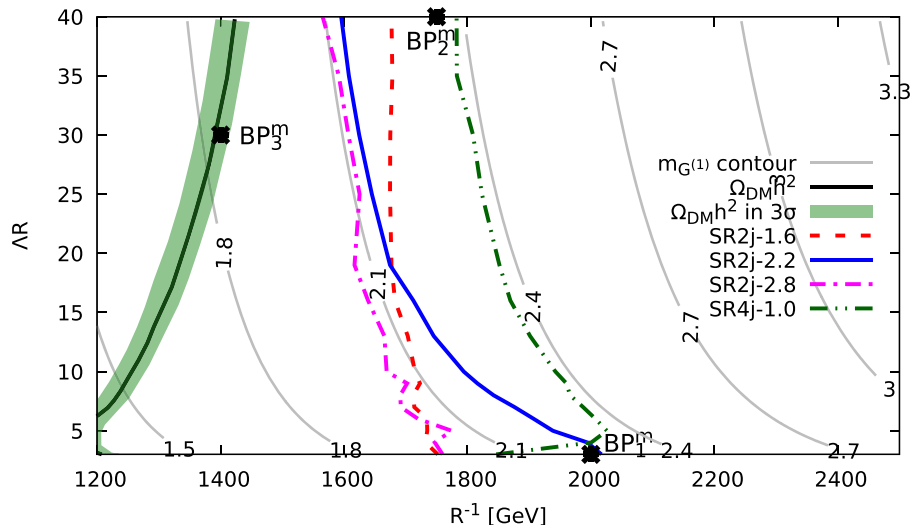


FIG. 1. 95% C.L. exclusion plot on R^{-1} - ΔR plane from different SRs (see Table I) of 13 TeV ATLAS search [84] for multijets + \cancel{E}_T with 139 fb^{-1} integrated luminosity data. The region to the left of the exclusion lines corresponding to different SRs is ruled out at 95% C.L. Level-one KK gluon mass ($m_{G^{(1)}}$) contours are laid over as gray lines, along with corresponding masses printed in TeV. The three benchmark points, listed in Table III, are also shown in filled black dots. The black solid line with green band of 3σ significance surrounding it represents the region that gives correct dark matter relic density [57]. The entire region to the right of the relic density ($\Omega_{\text{DM}} h^2$) curve is said to be ruled out in view of overclosure of the universe.

curve is ruled out at 95% C.L. Figure 1 also shows level-one KK gluon mass (in TeV) contours. For large ΔR , the strongest bound comes from four-jet final state (in particular, SR4j-1.0 signal region), which excludes level-one KK gluon mass below about 2.37 TeV. Note that the parameter space with lower $\Delta R \lesssim 5$ seems somewhat less restricted. For small ΔR , the strongest bound of about 2.22 TeV on level-one KK gluon mass results from SR2j-2.2. The numerical predictions for signal multijet + \cancel{E}_T cross sections in different SRs are presented in Table I for the mUED benchmark points defined in Table III. BP_1^m represents the part of mUED parameter space characterized by small $\Delta R \sim 3$ and hence a highly degenerate mass spectra for level-one KK particles. As a result, the decays of level-one quarks/gluons give rise to very soft jets at the LHC. For such a scenario, a monojetlike final state comprising a single high p_T jet, resulting primarily from initial state radiation, accompanied by missing transverse energy, is a promising channel. Table I shows that BP_1^m is excluded from SR2j-2.2, which is indeed a monojetlike [111,112] signal region. BP_2^m (BP_3^m) corresponds to large $\Delta R \sim 40$ (30) and hence relatively larger mass splittings between level-one KK particles. At the parton level, the pair (associated) production of level-one KK gluons (in association with level-one KK quarks) and their subsequent decays give rise to four (three) hard jets. Additional jets also arise from initial state radiation. Therefore, for large ΔR regions, four-jet channels (in particular, SR4j-1.0) are the most promising ones for estimating the bound, as can be seen from Table I as well as from Fig. 1.

Although we do not claim to have performed any dark matter related analysis, for the sake of completeness, we have shown the relic density bound on the R^{-1} - ΔR plane from Ref. [57]. The potential reason for its inclusion is that the bound from dark matter abundance appears to be the most severe one and strips off a large chunk of parameter space. In Fig. 1, the narrow green strip centered around the solid black line shows the parameter region with correct dark matter relic density. The band signifies the 3σ tolerance level. The parameter space on the left of the RD line results in relic densities that are smaller than the RD observed by WMAP/PLANCK. Therefore, this region is allowed in the sense that one can always concoct scenarios with multicomponent dark matter in order to evade such strict constraints from relic abundance. However, the entire region to the right of the relic density curve in Fig. 1 corresponds to relic densities larger than the WMAP/PLANCK result and hence is ruled out. Therefore, we can conclude from Fig. 1 that the region of the R^{-1} - ΔR plane, which is consistent with WMAP/PLANCK RD data, has already been ruled out by the ATLAS multijet + \cancel{E}_T searches at 13 TeV LHC with 139 fb^{-1} integrated luminosity. Hence, we shift our focus on the nonminimal UED, where an enhanced number of parameters offer rich phenomenology. The next section is slotted for discussion on the theoretical setup of the model.

IV. nmUED: MODEL DESCRIPTION

The assumption of vanishing boundary terms in mUED is somewhat unnatural, since they can anyway be generated at the loop level. Moreover, these boundary-localized terms

obey all the symmetries of the model [113]. The non-minimal version of the model (nmUED) takes these BLTs into account. Every boundary-localized term is associated with a parameter, which we generally denote by r . The presence of these unknown BLT parameters drastically alters the nmUED mass spectrum compared to the mUED one. Moreover, the interaction vertices of involving various nonzero KK modes are nontrivially modified by a multiplicative factor known as overlap integrals. However, before going into the collider phenomenology of the nmUED scenario, we briefly introduce the theoretical setup of the nmUED scenario.

The most general nmUED action is required to be invariant under the gauge symmetry of the SM, i.e., invariant under $SU(3)_C \times SU(2)_W \times U(1)_Y$, as well as the Lorentz symmetry in 4D, and can be written as

$$\mathcal{S}_{\text{nmUED}} = \mathcal{S}_{\text{gluon}} + \mathcal{S}_W + \mathcal{S}_B + \mathcal{S}_{\text{quark}} + \mathcal{S}_{\text{lepton}} + \mathcal{S}_{\text{scalar}}, \quad (4.1)$$

where the individual parts of the full nmUED action $\mathcal{S}_{\text{nmUED}}$ are discussed in the following. The gauge part of the action is given by

$$\begin{aligned} \mathcal{S}_{\text{gluon}} &= \int d^4x \int_0^{\pi R} dy \left\{ -\frac{1}{4} G_{MN}^a G^{aMN} + (\delta(y) + \delta(y - \pi R)) \left[-\frac{r_G}{4} G_{\mu\nu}^a G^{a\mu\nu} \right] \right\}, \\ \mathcal{S}_W &= \int d^4x \int_0^{\pi R} dy \left\{ -\frac{1}{4} W_{MN}^i W^{iMN} + (\delta(y) + \delta(y - \pi R)) \left[-\frac{r_W}{4} W_{\mu\nu}^i W^{i\mu\nu} \right] \right\}, \\ \mathcal{S}_B &= \int d^4x \int_0^{\pi R} dy \left\{ -\frac{1}{4} B_{MN} B^{MN} + (\delta(y) + \delta(y - \pi R)) \left[-\frac{r_B}{4} B_{\mu\nu} B^{\mu\nu} \right] \right\}, \end{aligned} \quad (4.2)$$

where G_{MN}^a , W_{MN}^i , and B_{MN} stand for 5D field-strength tensors corresponding to the $SU(3)_C$, $SU(2)_W$ and $U(1)_Y$ gauge fields, respectively. The symbols M and N run for 0, 1, 2, 3, 5 and the Greek indices run for 0, 1, 2, 3. The actions clearly consist of two parts. The first parts are the usual gauge kinetic term in 5D. The second parts are the brane (also called boundary)-localized kinetic

terms (BLKTs). These terms appear only at the boundaries of the brane and the bulk, as can be seen by the presence of delta functions. We consider boundary parameters at the two orbifold-fixed points to be the same, which ensures the conservation of KK parity. Now we briefly describe the fermionic parts of the action, which can be written as

$$\begin{aligned} \mathcal{S}_{\text{quark}} &= \sum_{j=1}^3 \int d^4x \int_0^{\pi R} dy \left[\bar{Q}_j i \Gamma^M \mathcal{D}_M Q_j + r_Q \{ \delta(y) + \delta(y - \pi R) \} \bar{Q}_j i \gamma^\mu \mathcal{D}_\mu P_L Q_j + \bar{U}_j i \Gamma^M \mathcal{D}_M U_j \right. \\ &\quad \left. + r_U \{ \delta(y) + \delta(y - \pi R) \} \bar{U}_j i \gamma^\mu \mathcal{D}_\mu P_R U_j + \bar{D}_j i \Gamma^M \mathcal{D}_M D_j + r_Q \{ \delta(y) + \delta(y - \pi R) \} \bar{D}_j i \gamma^\mu \mathcal{D}_\mu P_R D_j \right], \end{aligned} \quad (4.3)$$

$$\begin{aligned} \mathcal{S}_{\text{lepton}} &= \sum_{j=1}^3 \int d^4x \int_0^{\pi R} dy \left[\bar{L}_j i \Gamma^M \mathcal{D}_M L_j + r_L \{ \delta(y) + \delta(y - \pi R) \} \bar{L}_j i \gamma^\mu \mathcal{D}_\mu P_L L_j \right. \\ &\quad \left. + \bar{E}_j i \Gamma^M \mathcal{D}_M E_j + r_L \{ \delta(y) + \delta(y - \pi R) \} \bar{E}_j i \gamma^\mu \mathcal{D}_\mu P_R E_j \right], \end{aligned} \quad (4.4)$$

where 5D quark (lepton) doublet and singlets are denoted by $Q(L)$ and $U/D(E)$, respectively, $j = 1, 2, 3$ is the generation index, $\Gamma_M = (\gamma_\mu, i\gamma_5)$ denotes γ matrices in 5D, and \mathcal{D}_M is the gauge covariant derivative in 5D. Finally, the action corresponding to the 5D Higgs field is given by

$$\begin{aligned} \mathcal{S}_{\text{scalar}} &= \int d^4x \int_0^{\pi R} dy \left\{ (\mathcal{D}^M \Phi)^\dagger (\mathcal{D}_M \Phi) + \mu_5^2 \Phi^\dagger \Phi - \lambda_5 (\Phi^\dagger \Phi)^2 \right. \\ &\quad \left. + \{ \delta(y) + \delta(y + \pi R) \} (r_\Phi (\mathcal{D}^\mu \Phi)^\dagger (\mathcal{D}_\mu \Phi) + \mu_B^2 \Phi^\dagger \Phi - \lambda_B (\Phi^\dagger \Phi)^2) \right\}, \end{aligned} \quad (4.5)$$

where Φ is the 5D Higgs. μ_5 and λ_5 represent the 5D bulk Higgs mass parameter and scalar self-coupling, respectively. The BLKT parameter for the scalar field is r_Φ ; μ_B and λ_B are the boundary-localized Higgs mass parameter and the scalar quartic coupling, respectively. We must mention that all the BLT parameters (r_i where i stands for G , W , B , Q , L , and Φ fields) are dimensionful parameters. However, we express our results in Sec. IV A in terms of scaled BLT parameters $R_i = r_i R^{-1}$ as is customary.

The nmUED action written in the previous paragraph contains the information of the full theory in 5D. 5D fields can be expanded into x_μ and y dependent parts where x_μ is the usual 4D space-time coordinates and y is the extra dimension coordinate, which is compactified on a S_1/Z_2 orbifold. Once the mode expansions are fed into the actions and the extra-dimensional coordinate y is integrated out, we obtain a 4D effective theory involving the SM particles as well as their KK modes. For example, the mode expansions for the 5D gluon can be written as

$$G_\mu^{a(n)}(x, y) = \sum_{n=0}^{\infty} G_\mu^{a(n)}(x) f_G^{(n)}(y), \quad \text{with}$$

$$f_G^{(n)}(y) = N_{G^{(n)}} \times \begin{cases} \frac{\cos(m_{G^{(n)}} y)}{C_G} & \text{for } n \text{ even} \\ -\frac{\sin(m_{G^{(n)}} y)}{S_G} & \text{for } n \text{ odd,} \end{cases}$$

where $C_G = \cos(m_{G^{(n)}} \pi R/2)$ and $S_G = \sin(m_{G^{(n)}} \pi R/2)$. Note that the above expansion together with the boundary conditions gives rise to the following transcendental equations:

$$r_G m_{G^{(n)}} = \begin{cases} -2 \tan\left(\frac{m_{G^{(n)}} \pi R}{2}\right) & \text{for } n \text{ even} \\ 2 \cot\left(\frac{m_{G^{(n)}} \pi R}{2}\right) & \text{for } n \text{ odd.} \end{cases} \quad (4.6)$$

In the framework of nmUED, the mass of the n th level KK gluon ($m_{G^{(n)}}$) is obtained by solving these transcendental equations. The normalization of the wave function ($N_{G^{(n)}}$) is given by

$$N_{G^{(n)}} = \left[\left(\frac{\pi R}{2} \right) \left(1 + \frac{r_G^2 m_{G^{(n)}}^2}{4} + \frac{r_G}{\pi R} \right) \right]^{-\frac{1}{2}}. \quad (4.7)$$

Such KK decomposition and transcendental equations are common for all the 5D fields. Therefore, in nmUED scenario, the masses for the KK modes of other SM particles are also given by the solution of transcendental equations similar to those in Eq. (4.6) with appropriate BLT parameters.

It is interesting to note that the phenomenology of the level-one electroweak gauge sector of nmUED is significantly different from that of mUED since the masses and mixings of the level-one KK EW gauge bosons in nmUED nontrivially depend on the BLT parameters r_W , r_B , and r_Φ . In the context of mUED, the masses of the lightest (i.e., the LKP, which is the DM candidate in the theory) and next-to-lightest level-one KK gauge boson are determined by the radiative corrections. In addition, the extent of mixing between the level-one $U(1)_Y$ and $SU(2)_W$ KK gauge bosons is minuscule, unless R^{-1} is very small. Therefore, in mUED, the lightest and next-to-lightest

level-one KK gauge bosons are, for all practical purposes, essentially the level-one excitations of $U(1)_Y$ and $SU(2)_W$ gauge bosons, respectively. However, in the presence of the various overlap integrals involving the gauge and scalar BLT parameters, the mixing between the level-one $U(1)_Y$ and $SU(2)_W$ gauge bosons could be large in the framework of nmUED. Moreover, depending on the choice of r_W , r_B , and r_Φ , the LKP in nmUED could be either a level-one excitation of $U(1)_Y$ gauge boson or a level-one excitation of $SU(2)_W$ gauge boson. These facts, in turn, have profound implications for the dark matter phenomenology. Note that, in mUED, due to little freedom available for determining the mass spectrum and mixing, the observed value of dark matter RD provides a stringent upper bound on R^{-1} , which essentially rules out the model at the LHC. However, the additional parameters r_W , r_B , and r_Φ in nmUED play a crucial role to lift the RD upper bound on R^{-1} . It has been shown in Ref. [70] that, with proper choice of r_W and r_B , larger values of R^{-1} are possible without conflicting with the measured value of dark matter RD. The freedom in setting the mass spectrum of level-one KK particles at a required value also helps specific coannihilation channels to contribute more and thus obtain the required RD. We intend to address these issues related to the dark matter phenomenology of nmUED in a future article. In the present article, we focus on the collider bounds on the masses of level-one KK quarks and gluons in the framework of nmUED.

Before going into the collider phenomenology of nmUED, it is important to mention that the couplings, involving the zero-mode and nonzero-mode KK particles, are also modified nontrivially by factors known as the overlap integrals. These coupling modifications appear once we plug in the KK expansions in 5D Lagrangian and integrate over the extra-dimensional coordinate y . Note that a generic interaction of a level- l gauge boson ($V^{(l)}$) with a pair of level- m and k fermion-antifermion [$\Psi^{(m)}(x)$ and $\bar{\Psi}^{(k)}(x)$] results from the following term in the 5D action after compactifying the extra-dimensional coordinate y :

$$\begin{aligned} \mathcal{S}_{\text{int}} &= \tilde{g} \int d^4x \int dy \sum_{k,l,m} (\bar{\Psi}^{(k)}(x) f_\Psi^{(k)}(y)) \\ &\quad \times \gamma^\mu (V_\mu^{(l)}(x) f_V^{(l)}(y)) \times (\Psi^{(m)}(x) f_\Psi^{(m)}(y)) \\ &= \sum_{k,l,m} \int d^4x \tilde{g} \left[\int dy f_\Psi^{(k)}(y) f_V^{(l)}(y) f_\Psi^{(m)}(y) \right] \\ &\quad \times [\bar{\Psi}^{(k)}(x) \gamma^\mu V_\mu^{(l)}(x) \Psi^{(m)}(x)], \end{aligned}$$

where \tilde{g} is the corresponding gauge coupling in 5D. The connection between 5D gauge coupling \tilde{g} and its 4D counterpart is given by $g = \tilde{g}/\sqrt{r_V + \pi R}$, where r_V is the corresponding BLT parameter for the 5D gauge boson V_M . Note that the integration over the extra-dimensional coordinate y is nonzero only for certain combinations of

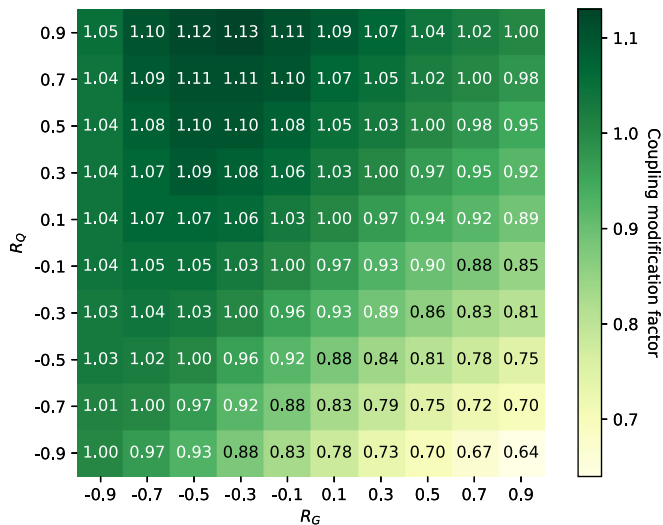


FIG. 2. The $Q^{(0)}G^{(1)}Q^{(1)}$ coupling modification factors are plotted against scaled BLT parameters R_G and R_Q corresponding to gluon and quark, respectively. The actual coupling for the $Q^{(0)}G^{(1)}Q^{(1)}$ vertex is given by these factors multiplied by the QCD coupling g_s .

the KK numbers (k, l, m) and hence acts as a selection rule known as KK number conservation, for interactions involving different KK-level particles. In mUED, the integration over the extra-dimensional coordinate in the above equation is either one (for KK number conserving interactions) or zero (for KK number violating interactions) depending on the choice of (k, l, m) . However, the presence of BLTs in nmUED result in a y profile of KK excitations, which is different from the mUED case and hence gives rise to nontrivial overlap integral. Depending on the values of the BLT parameters, the overlap integrals can enhance or reduce a particular coupling and thereby influence the phenomenology of the model. In Fig. 2, the modification factors for the gauge coupling involving a level-one KK gluon, a level-one KK quark, and a SM quark have been plotted against the gluon and quark scaled⁹ BLT parameters. Figure 2 shows significant deviation from unity in different parts of the R_G - R_Q plane. It can be deduced from Fig. 2 that, in certain parts of the R_G - R_Q plane, one could obtain an enhancement (suppression) as large as 13% (36%) in the interaction strength of the $Q^{(0)}G^{(1)}Q^{(1)}$ vertex compared to the interaction strength of pure QCD vertex.

A. Collider phenomenology

After discussing the nmUED model, mass spectrum, and coupling modifications, we are now equipped enough to

⁹From now on, we display our results in terms of dimensionless scaled BLT parameters defined as $R_i = r_i/R$ as defined earlier.

study its collider phenomenology and impose bounds from the ATLAS search for multijet plus \cancel{E}_T final states. However, before delving into the ATLAS analysis, it is important to discuss the productions of different KK particles and their subsequent decays in the framework of nmUED. The LHC being a proton-proton collider, we only consider the QCD pair productions of level-one KK quarks/gluons in our analysis. Unlike mUED,¹⁰ the nmUED QCD pair production cross sections of level-one KK particles are determined by radius of compactification as well as the BLT parameters for the quarks and gluons. The inverse of radius of compactification sets the overall mass scale for the level-one KK particles in nmUED, over which R_G and R_Q fix the masses of the KK gluons and KK quarks, respectively. In addition, the BLT parameters also govern the strength of interactions involving the SM and level-one KK particles, which are crucial for the productions as well as decays of the level-one KK particles. For example, the $Q^{(0)}G^{(1)}Q^{(1)}$ coupling (the dependence of which on R_G and R_Q is shown in Fig. 2) appears in all the relevant QCD production of level-one KK particles at the LHC, namely $G^{(1)}G^{(1)}$, $G^{(1)}Q^{(1)}/q^{(1)}$, $Q^{(1)}Q^{(1)}$, $Q^{(1)}\bar{Q}^{(1)}$, $q^{(1)}q^{(1)}$, $q^{(1)}\bar{q}^{(1)}$, etc. To illustrate the dependence of QCD productions of level-one KK particles on R_Q and R_G , we have presented the pair/associated production cross sections of level-one KK gluon and pair productions of level-one KK quarks in Figs. 3 and 4, respectively. The left panel of Fig. 3 shows the pair production cross sections of level-one KK gluons for fixed $m_{G^{(1)}} = 2$ TeV.¹¹ The dominant contribution¹² to the $G^{(1)}G^{(1)}$ production [$\sigma(pp \rightarrow G^{(1)}G^{(1)})$] at the LHC results from the gluon-gluon initiated process with a level-one KK gluon in the $t(u)$ channel. The vertices involved in the Feynman diagrams of $gg \rightarrow G^{(1)}G^{(1)}$ are purely QCD vertices that do not get modified, and hence

¹⁰In the framework of mUED, the pair and associated production cross sections of level-one KK quarks and KK gluons depend only on the masses $m_{Q^{(1)}}$ and $m_{G^{(1)}}$ and hence on R^{-1} and Λ .

¹¹In nmUED, the level-one KK gluon mass is obtained by solving the transcendental equation in Eq. (4.6), and hence $m_{G^{(1)}}$ depends on both R^{-1} and R_G . For a given value of R_G , one can obtain $m_{G^{(1)}} = 2$ TeV by suitably choosing a value for R^{-1} . Therefore, the plots in Fig. 3 (as well as the plots in Fig. 4) do not correspond to a particular value of R^{-1} . To clearly display the dependence of QCD cross sections on R_Q and R_G , one needs to minimize the dependence on parton densities and phase space factors and hence ensure fixed values for the final state particle masses. This motivates us to present the cross sections in Fig. 3 (Fig. 4) for a fixed $m_{G^{(1)}}(m_{Q^{(1)}})$ instead of a fixed R^{-1} .

¹²Quark-antiquark initiated diagrams also contribute to $\sigma(pp \rightarrow G^{(1)}G^{(1)})$. Gluon densities being larger than quark/antiquark densities at the LHC energies, the quark-antiquark initiated contributions to $\sigma(pp \rightarrow G^{(1)}G^{(1)})$ are suppressed compared to the gluon-fusion contribution.

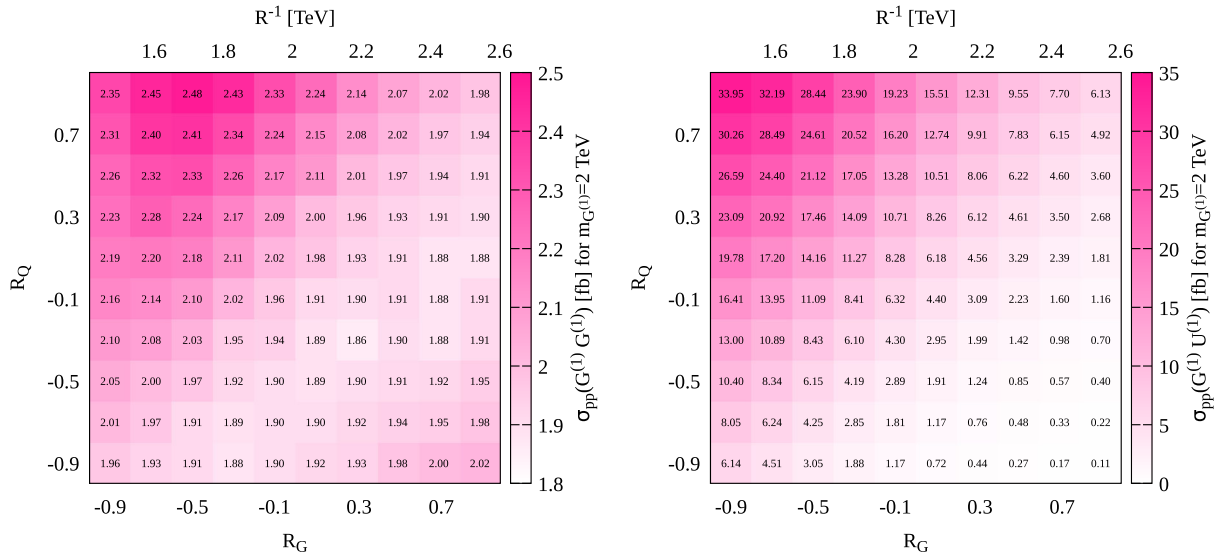


FIG. 3. Cross sections (in femtobarn) for the pair (left) and associated (right) production level-one KK gluon are presented on the R_G - R_Q plane for the LHC at 13 TeV center-of-mass energy. Instead of fixing R^{-1} , the level-one KK gluon mass is kept fixed at $m_{G^{(1)}} = 2$ TeV. The x_2 axis shows the values of R^{-1} .

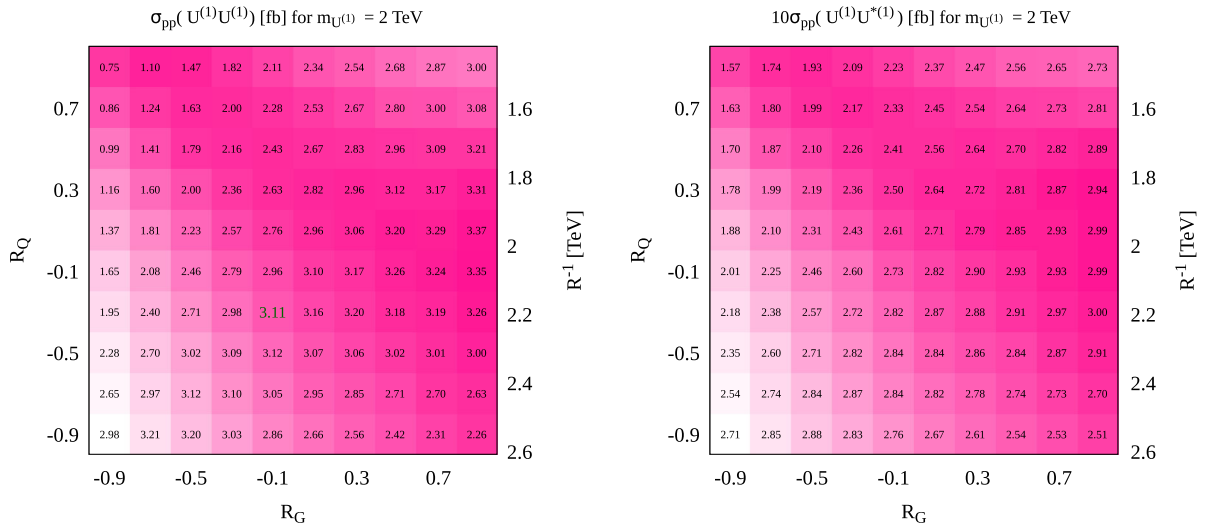


FIG. 4. Cross sections (in femtobarn) for the up-type level-one quark-quark (left) and quark-antiquark (right) pair productions are presented on R_G - R_Q plane for the LHC at 13 TeV center-of-mass energy. Instead of fixing R^{-1} , the level-one KK quark mass is kept fixed at $m_{U^{(1)}} = 2$ TeV. The y_2 axis shows the variation of R^{-1} .

$\sigma(gg \rightarrow G^{(1)}G^{(1)})$ depends only on $m_{G^{(1)}}$. However, some of the Feynman diagrams [in particular, the $t(u)$ channel level-one KK quark exchange diagrams] for the subdominant $q\bar{q} \rightarrow G^{(1)}G^{(1)}$ production channel involve the $Q^{(0)}G^{(1)}Q^{(1)}$ vertex, which gets modified. Therefore, the variation of $\sigma(pp \rightarrow G^{(1)}G^{(1)})$ in Fig. 3 (left panel) results from the R_G and R_Q dependence of quark-antiquark initiated contribution to the total cross section. An important fact is that the two Feynman diagrams, namely the s -channel gluon exchange diagram and $t(u)$ -channel $Q^{(1)}$ exchange diagram, contributing to the quark-antiquark

initiated production of $G^{(1)}$ pairs, interfere destructively. For a given R_G (and hence fixed R^{-1}) in Fig. 2, increasing R_Q corresponds to decreasing $m_{Q^{(1)}}$ and hence stronger destructive interference, which tends to decrease the cross section. On the other hand, the coupling modification factors increase with increasing R_Q (see Fig. 2), which tends to increase the cross section. These two competing factors explain the pattern of $\sigma(pp \rightarrow G^{(1)}G^{(1)})$ variation on R_Q and R_G as displayed in Fig. 3 (left panel).

The associated production cross section [$\sigma(pp \rightarrow G^{(1)}U^{(1)})$] of a level-one KK gluon in association with a

TABLE IV. nmUED benchmark points and mass spectra of relevant level-one KK particles.

BPs	R^{-1} (TeV)	(R_Q, R_G)	$m_{G^{(1)}} (TeV)$	$m_{Q^{(1)}} (TeV)$	$m_{W^{(1)}} (TeV)$	$m_{Z^{(1)}} (TeV)$	$m_{L^{(1)}} (TeV)$	$m_{B^{(1)}} (TeV)$
BP ₁ ^{nm}	1.9	(-0.9, -0.1)	1.963	2.559	1.913	1.914	1.906	1.900
BP ₂ ^{nm}	2.1	(-0.1, -0.1)	2.169	2.169	2.114	2.115	2.107	2.100
BP ₃ ^{nm}	2.0	(-0.3, -0.7)	2.531	2.209	2.013	2.015	2.007	2.000

level-one up-type KK quark¹³ as a function of R_G and R_Q is presented in Fig. 3 (right panel) for fixed $G^{(1)}$ mass of 2 TeV. Here, the mass of the level-one up-type KK quark, however, is not constant over the R_G - R_Q plane. At the LHC, the $G^{(1)}U^{(1)}$ associated production is a quark-gluon initiated process that proceeds via the exchange of a level-one KK quark or KK gluon in the $t(u)$ channel. The large variation of $\sigma(pp \rightarrow G^{(1)}U^{(1)})$ in Fig. 3 (right panel) mainly occurs due to the variation of the level-one KK quark mass in the final state, although both the Feynman diagrams contributing to $\sigma(pp \rightarrow G^{(1)}U^{(1)})$ contain coupling that depends on BLT parameters.

The R_G - R_Q dependence of the production cross sections of level-one KK quark-quark pair ($\sigma(pp \rightarrow U^{(1)}U^{(1)})$) and KK quark-antiquark pair [$\sigma(pp \rightarrow U^{(1)}\bar{U}^{(1)})$] are presented in the left and right panels, respectively, of Fig. 4 for $m_{U^{(1)}} = 2$ TeV. In order to generate a fixed level-one KK quark mass, R^{-1} needs to be varied with R_Q . The variation of R^{-1} is also depicted as the y_2 axis in Fig. 4. The dominant contribution to $\sigma(pp \rightarrow U^{(1)}U^{(1)})$ comes from the quark-quark fusion process at the LHC through a level-one KK gluon in the $t(u)$ channel. The resulting variation of $\sigma(pp \rightarrow U^{(1)}U^{(1)})$ with respect to R_G - R_Q is shown in Fig. 4 (left panel). On the other hand, $\sigma(pp \rightarrow U^{(1)}\bar{U}^{(1)})$ receives contributions from quark-antiquark and gluon-gluon initiated processes. While the gluon-gluon initiated channel depends only on $m_{U^{(1)}}$ and hence is independent of R_G and R_Q for a fixed $m_{U^{(1)}} = 2$ TeV, the mild variation of $\sigma(pp \rightarrow U^{(1)}\bar{U}^{(1)})$ over the R_G - R_Q plane (see the right panel of Fig. 4) results from the subdominant quark-antiquark initiated process.

After discussing the productions of level-one KK quarks/gluons, we will now discuss the decays of various level-one KK particles and the resulting signatures at the LHC. Mass hierarchy among various KK particles plays a crucial role in determining the decay cascades of level-one KK quarks/gluons and hence the topology and kinematics of the final states at the LHC. While, for mUED, the mass hierarchy

¹³At the LHC, the electroweak productions of level-one KK quarks/gluons are negligible compared to the QCD productions. Therefore, we have neglected EW productions of level-one quarks/gluons in our analysis. Note that QCD cannot distinguish between u-type and d-type or singlet and doublet KK quarks. Therefore, the cross sections presented here are valid for both singlet and doublet up-type quarks. Results will be different for level-one down-type quarks due to the parton density of $d(\bar{d})$ quark.

among KK particles of a given level is completely determined by the radiative corrections, the nmUED mass spectrum is determined by the BLT parameters, which are free parameters of the theory. For example, $R_G < R_Q$ would render a mass hierarchy similar to mUED with KK gluon being more massive than KK quarks, while $R_G > R_Q$ results in KK quarks being heavier than the KK gluons. In order to discuss the decays and the resulting collider signatures nmUED, as well as present the numerical results, we have chosen three benchmark points listed in Table IV along with the masses of relevant level-one KK particles. The BPs in Table IV are characterized by R^{-1} and (R_Q, R_G) . We have assumed fixed values for the BLT parameters¹⁴ in the EW sector, namely R_W, R_Φ, R_B , and R_L . We consider $R_W = -0.02 = R_\Phi$ and set R_B to zero. This particular choice of the EW BLT parameters gives rise to a LKP that is dominantly the level-one KK excitation of the $U(1)_Y$ gauge boson ($B^{(1)}$) with significant mixing with the level-one KK excitation of the neutral $SU(2)_L$ gauge boson ($W^{3(1)}$). Note that the EW level-one KK gauge sector is highly degenerate (see Table IV) with the dominantly $SU(2)_L$ level-one KK gauge bosons, namely $W^{\pm(1)}$ and $Z^{(1)}$, being slightly heavier than the LKP. It has been shown in Ref. [70] that such an EW level-one sector of nmUED enhances the dark matter annihilation/coannihilation cross sections and hence allows larger values of R^{-1} without conflicting with the WMAP/PLANCK measured value of the RD. We have also fixed the BLT parameters for leptons at $R_L = -0.01$ and scanned over negative¹⁵ values of R_Q and R_G .

For $R_G < R_Q$ with $m_{G^{(1)}} > m_{Q^{(1)}}$ (see BP₃^{nm} in Table IV), the level-one KK gluon decays primarily to a SM quark and its level-one KK counterpart. Since the decays of level-one KK quarks into a SM quark and $G^{(1)}$ are kinematically forbidden for BP₃^{nm}, $m_{Q^{(1)}} > m_{W^{(1)}}/m_{B^{(1)}}$, usually result in a level-one doublet KK quark decaying to a SM quark in association with a $W^{(1)\pm}/Z^{(1)}/B^{(1)}$. Note that for the

¹⁴It is important to mention the existing constraints on the BLT parameters. The absence of any tachyonic modes requires the scaled BLT parameters to be larger than $-\pi$. The presence of BLTs leads to the KK number violation at the tree level. The LHC searches for Z' in dilepton channels lead to stringent constraints on the production of level-two gauge bosons via KK number violating couplings involving a level-two gauge boson and a pair of SM fermions. In particular, $R_{W/B} > 0.2$ for $R^{-1} = 1.5$ TeV [70] has already been excluded from the dilepton resonance searches at the LHC.

¹⁵For $R_B = 0$, positive values of R_Q or R_G give rise to a stable colored particle in the theory and are hence excluded.

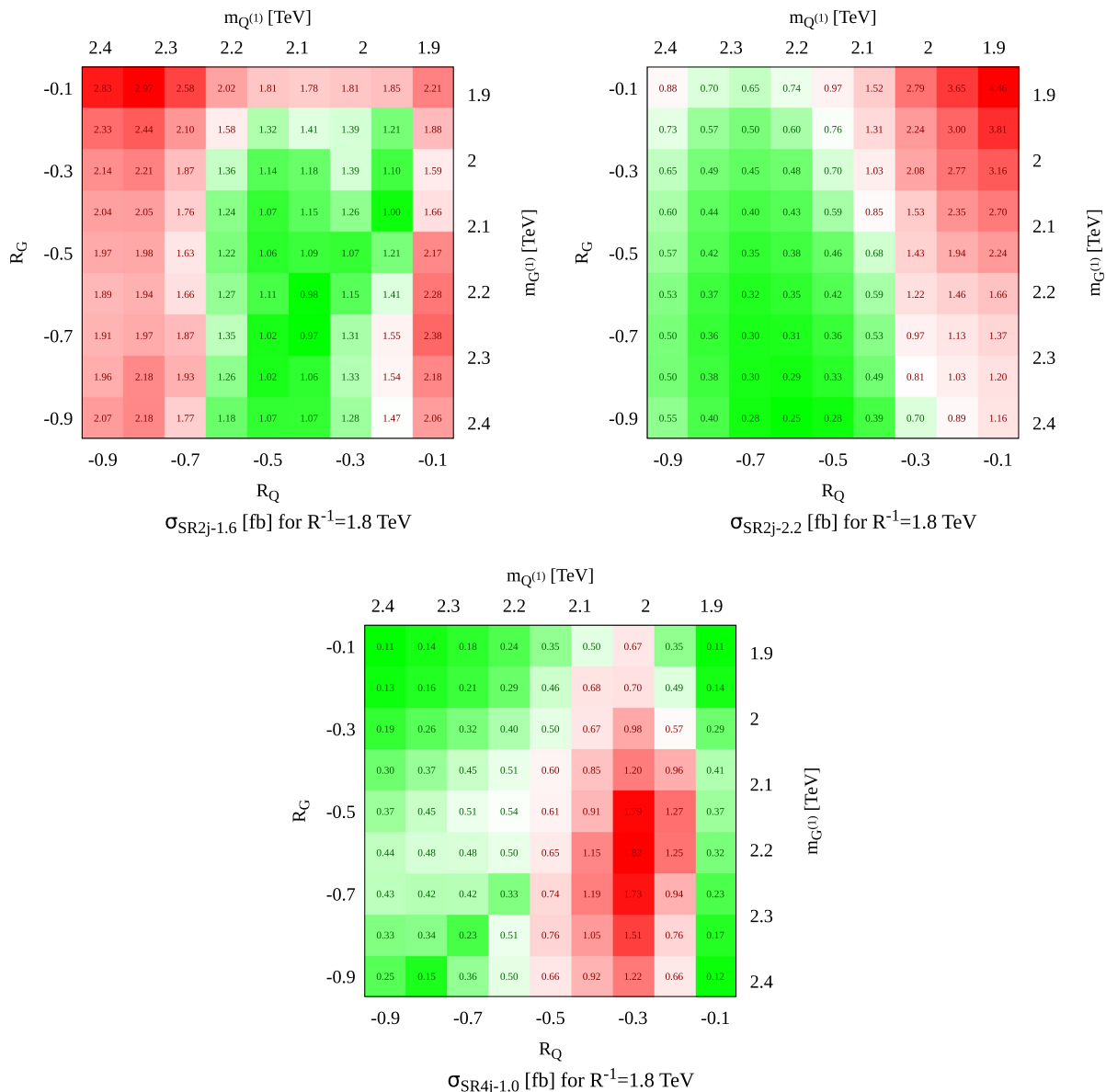


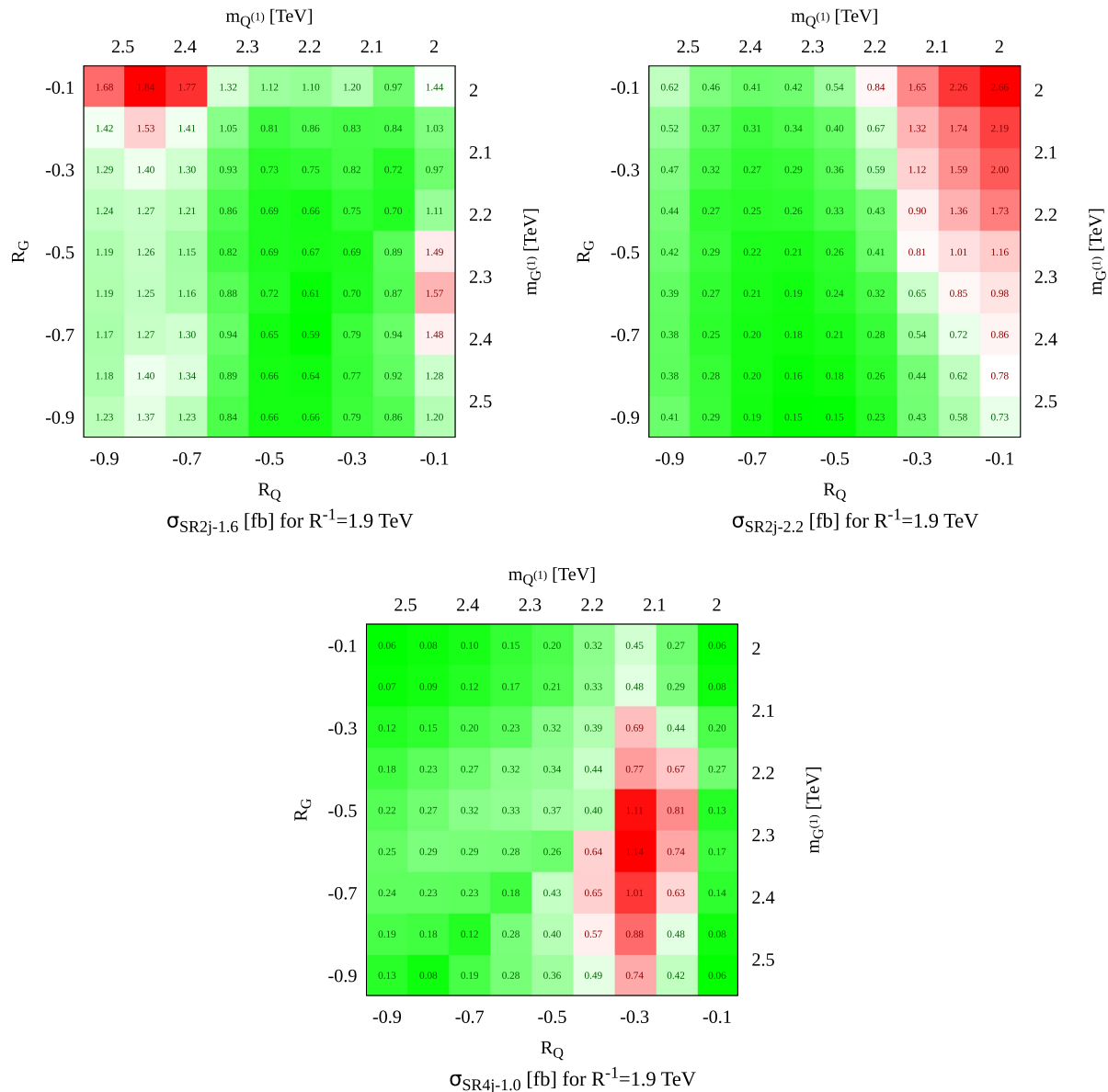
FIG. 5. Theoretical predictions for the visible cross sections in SR2j-1.6 (top left), SR2j-2.2 (top right), and SR4j-1.0 (bottom) SRs are presented as a function of R_Q (x_1 axis) and R_G (y_1 axis) for nmUED scenario with $R^{-1} = 1.8$ TeV, $R_{W(\Phi)} = -0.02$, $R_L = -0.01$, and $R_B = 0.0$. The level-one KK quark and KK gluon masses are also presented as x_2 axis and y_2 axis, respectively. For each of the signal regions, the excluded and allowed parts of parameter space are represented by red and green cells, respectively.

level-one singlet KK quarks, the decay into $W^{(1)\pm}$ is highly suppressed. In the scenario with $R_G > R_Q$ (see BP_1^{nm} in Table IV), the level-one KK quarks, being heavier than $G^{(1)}$, dominantly decay into a SM quark in association with a level-one KK gluon. On the contrary, $G^{(1)}$ undergoes a tree-level three-body decay via an off shell $Q^{(1)}$ into a SM quark-antiquark pair in association with a level-one EW boson ($W^{(1)\pm}/Z^{(1)}/B^{(1)}$). The level-one KK EW bosons subsequently decay into a pair of SM leptons and the LKP. The leptons arising from the decay of $W^{(1)\pm}/Z^{(1)}$ are usually very soft and hence often remain invisible at the LHC detectors. Therefore, the pair/associated productions of

level-one KK quarks and KK gluons give rise to multijet in association with large missing transverse energy final states, which will be discussed in the following in the context of a recent ATLAS search [84] for multijet + missing transverse energy final states at the LHC at 13 TeV center-of-mass energy and 139 fb^{-1} integrated luminosity.

The pair and associated productions of level-one KK quarks and KK gluons are generated in MADGRAPH.¹⁶ The

¹⁶Note that nmUED UFO files, which are required for generating nmUED events in MADGRAPH, are not available in the literature. We have implemented the nmUED model in FEYNRULES2.0 [114] to generate the UFO files.


 FIG. 6. Same as Fig. 5 for $R^{-1} = 1.9$ TeV.

MADGRAPH generated events are fed into PYTHIA8.2 for simulating decays, ISR, FSR, and hadronization. We use our own analysis code for the object reconstructions and computation of nmUED contributions to the multijet + \cancel{E}_T cross sections in different SRs defined by the ATLAS Collaboration [84] (see Sec. 2 and Table I). The nmUED predictions for the visible cross sections for the benchmark points (listed in Table IV) are presented in Table I. Figures 5 and 6 show the visible cross sections in signal regions SR2j-1.6 (top left panel), SR2j-2.2 (top right panel), and SR4j-1.0 (bottom panel) as a function of R_Q and R_G for $R^{-1} = 1.8$ TeV (Fig. 5) and 1.9 TeV (Fig. 6). Clearly, the reddish cells of Figs. 5 and 6 correspond to nmUED cross sections, which are larger than the ATLAS observed 95% C.L. upper bound on $\langle \epsilon\sigma \rangle_{\text{obs}}^{95}$ (see Table I) in the respective

signal regions, and hence the corresponding parameter points are ruled out.

The complementarity of SRs is clearly visible in Fig. 5. While SR2j-2.2 and SR2j-1.6 signal regions are more effective to probe the low (represented by BP_1^{nm}) and high (represented by BP_2^{nm}) R_Q regions, respectively, the intermediate (represented by BP_3^{nm}) R_Q region is susceptible to SR4j-1.0 (see Figs. 5 and 6 and Table I). This particular pattern of the effectiveness of different SRs in different parts of the R_Q - R_G plane can be understood from the characteristics of multijet + \cancel{E}_T signatures in different parts of the R_Q - R_G plane. For example, the region characterized by higher values for both R_Q and R_G (top right corner of R_Q - R_G plane and represented by BP_2^{nm}) gives rise to a nmUED scenario with nearly degenerate masses for the

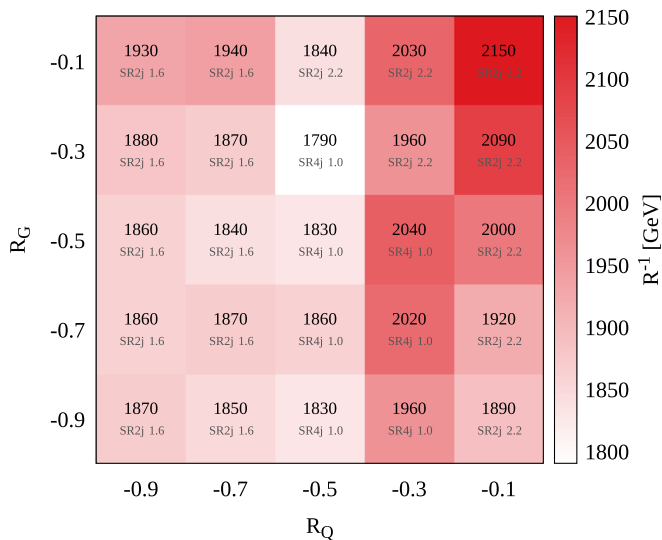


FIG. 7. The lower bounds on R^{-1} are presented as function of R_Q and R_G . The signal region that leads to a particular lower bound on R^{-1} for a given R_Q and R_G is also specified in the figure.

level-one quarks, gluons, and the LKP (see Table IV). Although the pair and associated production cross sections of $G^{(1)}$ and $Q^{(1)}$ in this region are large, the final state jets are usually too soft to pass the preselection criteria. The production of $G^{(1)}$ and $Q^{(1)}$ in association with a hard ISR jet gives rise to a monojet + \cancel{E}_T signature. It has already been discussed in the context of mUED phenomenology that the selection criteria of SR2j-2.2 is essentially a monojetlike selection criteria and hence is effective to probe this part of the R_Q - R_G plane. On the other hand, in the region characterized by low R_Q and/or low R_G (represented by BP_1^{nm} and BP_3^{nm} in Table IV), the level-one quarks and/or gluons are sufficiently heavy compared to the LKP and hence give rise to hard jets at the LHC. While the pair production of $G^{(1)}$ leads to four hard jets at parton level, two hard jets arise from the pair production of $Q^{(1)}$. Therefore, this part of the R_Q - R_G plane is susceptible to both SR2j-1.6 and SR4j-1.0. However, our analysis shows that SR2j-1.6 is more efficient to probe this region.

While all parts of the R_Q - R_G plane are ruled out from complementary signal regions for $R^{-1} = 1.8$ TeV (see Fig. 5), the ATLAS multijet search can probe only some part of the R_Q - R_G plane for $R^{-1} = 1.9$ TeV (see Fig. 6). Our final results are summarized in Fig. 7, which shows the

lower bounds on R^{-1} in different parts of the R_Q - R_G plane. The signal regions that lead to those lower bounds are also presented in Fig. 7. For $(R_Q, R_G) = (-0.1, -0.1)$, R^{-1} below 2.15 TeV is ruled out from SR2j-2.2, whereas the bound on R^{-1} could be as low as 1.79 TeV for $(R_Q, R_G) = (-0.5, -0.3)$.

V. SUMMARY AND CONCLUSION

To summarize, we have studied one universal extra dimension scenario against the dataset recorded by the ATLAS Collaboration in proton-proton collisions at a center-of-mass energy $\sqrt{s} = 13$ TeV, corresponding to an integrated luminosity of 139 fb^{-1} . The phenomenology of the minimal version of UED is completely determined by the two new parameters: namely the compactification radius R and the cutoff scale Λ . Our study clearly shows that mUED parameter space is completely ruled out by the ATLAS multijet + \cancel{E}_T analysis together with the dark matter relic density data. Next, we bring in boundary-localized terms (with R_G and R_Q as BLT parameters for gluon and quark fields, respectively) as an extension of mUED, called nonminimal UED. The introduction of such terms alters the phenomenology substantially. Mass spectrum in nmUED is determined by the transcendental equations coming from the boundary terms. Some interaction vertices are also altered as a result of the integration of extra-dimensional mode functions of the concerned particles. We have discussed strong production cross sections for the variations of the gluon and quark BLT parameters. We have performed a detailed cut-based analysis emulating the ATLAS multijet + \cancel{E}_T channel. Excluded regions of nmUED parameter space are shown in terms of R^{-1} , R_G , and R_Q .

ACKNOWLEDGMENTS

T. J. thanks Ipsita Saha, Sujoy Shil, Nabanita Ganguly, Sanchari Bhattacharyya, and Tisa Biswas for important discussions and much technical help regarding collider part. T. J. also thanks Swagata Ghosh for discussion regarding FEYNRULES. The authors acknowledge that the simulations and computations were supported in part by the SAMKHYA: High Performance Computing Facility provided by Institute of Physics, Bhubaneswar. K. G. acknowledges the support from the DST/INSPIRE Research Grant No. DST/INSPIRE/04/2014/002158 and SERB Core Research Grant No. CRG/2019/006831.

- [1] G. Aad *et al.* (ATLAS Collaboration), Observation of a new particle in the search for the Standard Model Higgs boson with the ATLAS detector at the LHC, *Phys. Lett. B* **716**, 1 (2012).
- [2] S. Chatrchyan *et al.* (CMS Collaboration), Observation of a new boson at a mass of 125 GeV with the CMS experiment at the LHC, *Phys. Lett. B* **716**, 30 (2012).
- [3] N. Arkani-Hamed, S. Dimopoulos, and G. Dvali, The hierarchy problem and new dimensions at a millimeter, *Phys. Lett. B* **429**, 263 (1998).
- [4] N. Arkani-Hamed, S. Dimopoulos, and G. Dvali, Phenomenology, astrophysics and cosmology of theories with submillimeter dimensions and TeV scale quantum gravity, *Phys. Rev. D* **59**, 086004 (1999).
- [5] L. Randall and R. Sundrum, A Large Mass Hierarchy from a Small Extra Dimension, *Phys. Rev. Lett.* **83**, 3370 (1999).
- [6] L. Randall and R. Sundrum, An Alternative to Compactification, *Phys. Rev. Lett.* **83**, 4690 (1999).
- [7] K. R. Dienes, E. Dudas, and T. Gherghetta, Neutrino oscillations without neutrino masses or heavy mass scales: A higher dimensional seesaw mechanism, *Nucl. Phys. B* **557**, 25 (1999).
- [8] K. R. Dienes, E. Dudas, and T. Gherghetta, Extra space-time dimensions and unification, *Phys. Lett. B* **436**, 55 (1998).
- [9] N. Arkani-Hamed and M. Schmaltz, Hierarchies without symmetries from extra dimensions, *Phys. Rev. D* **61**, 033005 (2000).
- [10] I. Antoniadis, A possible new dimension at a few TeV, *Phys. Lett. B* **246**, 377 (1990).
- [11] T. Appelquist, H.-C. Cheng, and B. A. Dobrescu, Bounds on universal extra dimensions, *Phys. Rev. D* **64**, 035002 (2001).
- [12] H.-C. Cheng, K. T. Matchev, and M. Schmaltz, Bosonic supersymmetry? Getting fooled at the CERN LHC, *Phys. Rev. D* **66**, 056006 (2002).
- [13] N. Arkani-Hamed, H.-C. Cheng, B. A. Dobrescu, and L. J. Hall, Self-breaking of the standard model gauge symmetry, *Phys. Rev. D* **62**, 096006 (2000).
- [14] G. Servant and T. M. Tait, Is the lightest Kaluza-Klein particle a viable dark matter candidate?, *Nucl. Phys. B* **650**, 391 (2003).
- [15] M. Kakizaki, S. Matsumoto, and M. Senami, Relic abundance of dark matter in the minimal universal extra dimension model, *Phys. Rev. D* **74**, 023504 (2006).
- [16] K. R. Dienes, E. Dudas, and T. Gherghetta, Grand unification at intermediate mass scales through extra dimensions, *Nucl. Phys. B* **537**, 47 (1999).
- [17] T. Appelquist, B. A. Dobrescu, E. Ponton, and H.-U. Yee, Proton Stability in Six Dimensions, *Phys. Rev. Lett.* **87**, 181802 (2001).
- [18] B. A. Dobrescu and E. Poppitz, Number of Fermion Generations Derived from Anomaly Cancellation, *Phys. Rev. Lett.* **87**, 031801 (2001).
- [19] T. G. Rizzo, Probes of universal extra dimensions at colliders, *Phys. Rev. D* **64**, 095010 (2001).
- [20] C. Macesanu, C. McMullen, and S. Nandi, Collider implications of universal extra dimensions, *Phys. Rev. D* **66**, 015009 (2002).
- [21] A. Muck, A. Pilaftsis, and R. Ruckl, Probing minimal 5-D extensions of the standard model: From LEP to an e⁺e⁻ linear collider, *Nucl. Phys. B* **687**, 55 (2004).
- [22] G. Bhattacharyya, P. Dey, A. Kundu, and A. Raychaudhuri, Probing universal extra dimension at the international linear collider, *Phys. Lett. B* **628**, 141 (2005).
- [23] M. Battaglia, A. Datta, A. De Roeck, K. Kong, and K. T. Matchev, Contrasting supersymmetry and universal extra dimensions at the clic multi-TeV e⁺e⁻ collider, *J. High Energy Phys.* **07** (2005) 033.
- [24] B. Bhattacharjee and A. Kundu, The international linear collider as a Kaluza-Klein factory, *Phys. Lett. B* **627**, 137 (2005).
- [25] A. Datta, K. Kong, and K. T. Matchev, Discrimination of supersymmetry and universal extra dimensions at hadron colliders, *Phys. Rev. D* **72**, 096006 (2005); Erratum, *Phys. Rev. D* **72**, 119901 (2005).
- [26] A. Datta, G. L. Kane, and M. Toharia, Is it SUSY?, [arXiv: hep-ph/0510204](https://arxiv.org/abs/hep-ph/0510204).
- [27] B. A. Dobrescu, D. Hooper, K. Kong, and R. Mahbubani, Spinless photon dark matter from two universal extra dimensions, *J. Cosmol. Astropart. Phys.* **10** (2007) 012.
- [28] A. Freitas and K. Kong, Two universal extra dimensions and spinless photons at the ILC, *J. High Energy Phys.* **02** (2008) 068.
- [29] K. Ghosh and A. Datta, Phenomenology of spinless adjoints in two universal extra dimensions, *Nucl. Phys. B* **800**, 109 (2008).
- [30] K. Ghosh and A. Datta, Probing two universal extra dimensions at international linear collider, *Phys. Lett. B* **665**, 369 (2008).
- [31] D. Choudhury, A. Datta, and K. Ghosh, Deciphering universal extra dimension from the top quark signals at the CERN LHC, *J. High Energy Phys.* **08** (2010) 051.
- [32] B. Bhattacharjee and K. Ghosh, Search for the minimal universal extra dimension model at the LHC with $\sqrt{s} = 7$ TeV, *Phys. Rev. D* **83**, 034003 (2011).
- [33] K. Ghosh, S. Mukhopadhyay, and B. Mukhopadhyaya, Discrimination of low missing energy look-alikes at the LHC, *J. High Energy Phys.* **10** (2010) 096.
- [34] G. Bertone, K. Kong, R. Ruiz de Austri, and R. Trotta, Global fits of the minimal universal extra dimensions scenario, *Phys. Rev. D* **83**, 036008 (2011).
- [35] H. Murayama, M. M. Nojiri, and K. Tobioka, Improved discovery of a nearly degenerate model: MUED using MT2 at the LHC, *Phys. Rev. D* **84**, 094015 (2011).
- [36] K. Nishiwaki, K.-y. Oda, N. Okuda, and R. Watanabe, Heavy Higgs at tevatron and LHC in universal extra dimension models, *Phys. Rev. D* **85**, 035026 (2012).
- [37] D. Choudhury, A. Datta, D. K. Ghosh, and K. Ghosh, Exploring two universal extra dimensions at the CERN LHC, *J. High Energy Phys.* **04** (2012) 057.
- [38] T. Flacke and C. Pasold, Constraints on split-UED from electroweak precision tests, *Phys. Rev. D* **85**, 126007 (2012).
- [39] K. Ghosh and K. Huitu, Constraints on universal extra dimension models with gravity mediated decays from ATLAS diphoton search, *J. High Energy Phys.* **06** (2012) 042.
- [40] G.-Y. Huang, K. Kong, and S. C. Park, Bounds on the fermion-bulk masses in models with universal extra dimensions, *J. High Energy Phys.* **06** (2012) 099.

- [41] G. Belanger, A. Belyaev, M. Brown, M. Kakizaki, and A. Pukhov, Testing minimal universal extra dimensions using Higgs boson searches at the LHC, *Phys. Rev. D* **87**, 016008 (2013).
- [42] T. Flacke, A. Menon, and Z. Sullivan, Constraints on UED from W' searches, *Phys. Rev. D* **86**, 093006 (2012).
- [43] A. Belyaev, M. Brown, J. Moreno, and C. Papineau, Discovering minimal universal extra dimensions (MUED) at the LHC, *J. High Energy Phys.* **06** (2013) 080.
- [44] L. Edelhäuser, T. Flacke, and M. Krämer, Constraints on models with universal extra dimensions from dilepton searches at the LHC, *J. High Energy Phys.* **08** (2013) 091.
- [45] T. Kakuda, K. Nishiwaki, K.-y. Oda, and R. Watanabe, Universal extra dimensions after Higgs discovery, *Phys. Rev. D* **88**, 035007 (2013).
- [46] U. K. Dey and A. Raychaudhuri, KK-number non-conserving decays: Signal of $n = 2$ excitations of extra-dimensional models at the LHC, *Nucl. Phys.* **B893**, 408 (2015).
- [47] J. Beuria, A. Datta, D. Debnath, and K. T. Matchev, LHC collider phenomenology of minimal universal extra dimensions, *Comput. Phys. Commun.* **226**, 187 (2018).
- [48] K. Ghosh, D. Karabacak, and S. Nandi, Universal extra dimension models with gravity mediated decays after LHC run II data, *Phys. Lett. B* **788**, 388 (2019).
- [49] K. Kong, S. C. Park, and T. G. Rizzo, A vector-like fourth generation with a discrete symmetry from split-UED, *J. High Energy Phys.* **07** (2010) 059.
- [50] C.-R. Chen, M. M. Nojiri, S. C. Park, J. Shu, and M. Takeuchi, Dark matter and collider phenomenology of split-UED, *J. High Energy Phys.* **09** (2009) 078.
- [51] S. C. Park and J. Shu, Split universal extra dimensions and dark matter, *Phys. Rev. D* **79**, 091702 (2009).
- [52] F. del Aguila, M. Perez-Victoria, and J. Santiago, Bulk fields with general brane kinetic terms, *J. High Energy Phys.* **02** (2003) 051.
- [53] M. Carena, T. M. Tait, and C. Wagner, Branes and orbifolds are opaque, *Acta Phys. Pol. B* **33**, 2355 (2002), <https://www.actaphys.uj.edu.pl/fulltext?series=Reg&vol=33&page=2355>.
- [54] H.-C. Cheng, K. T. Matchev, and M. Schmaltz, Radiative corrections to Kaluza-Klein masses, *Phys. Rev. D* **66**, 036005 (2002).
- [55] D. Choudhury and K. Ghosh, Bounds on universal extra dimension from LHC run I and II data, *Phys. Lett. B* **763**, 155 (2016).
- [56] N. Deutschmann, T. Flacke, and J. S. Kim, Current LHC constraints on minimal universal extra dimensions, *Phys. Lett. B* **771**, 515 (2017).
- [57] J. M. Cornell, S. Profumo, and W. Shepherd, Dark matter in minimal universal extra dimensions with a stable vacuum and the “right” Higgs boson, *Phys. Rev. D* **89**, 056005 (2014).
- [58] E. Komatsu *et al.* (WMAP Collaboration), Seven-year Wilkinson microwave anisotropy probe (WMAP) observations: Cosmological interpretation, *Astrophys. J. Suppl. Ser.* **192**, 18 (2011).
- [59] P. Ade *et al.* (Planck Collaboration), Planck 2015 results. XIII. Cosmological parameters, *Astron. Astrophys.* **594**, A13 (2016).
- [60] T. Flacke, A. Menon, and D. J. Phalen, Non-minimal universal extra dimensions, *Phys. Rev. D* **79**, 056009 (2009).
- [61] A. Datta, K. Nishiwaki, and S. Niyogi, Non-minimal universal extra dimensions: The strongly interacting sector at the large hadron collider, *J. High Energy Phys.* **11** (2012) 154.
- [62] T. Flacke, K. Kong, and S. C. Park, 126 GeV Higgs in next-to-minimal universal extra dimensions, *Phys. Lett. B* **728**, 262 (2014).
- [63] A. Datta, K. Nishiwaki, and S. Niyogi, Non-minimal universal extra dimensions with brane local terms: The top quark sector, *J. High Energy Phys.* **01** (2014) 104.
- [64] T. Flacke, K. Kong, and S. C. Park, Phenomenology of universal extra dimensions with bulk-masses and brane-localized terms, *J. High Energy Phys.* **05** (2013) 111.
- [65] A. Shaw, Status of exclusion limits of the KK-parity non-conserving resonance production with updated 13 TeV LHC, *Acta Phys. Pol. B* **49**, 1421 (2018).
- [66] A. Datta, U. K. Dey, A. Raychaudhuri, and A. Shaw, Universal extra-dimensional models with boundary terms: Probing at the LHC, *Nucl. Phys. B, Proc. Suppl.* **251–252**, 39 (2014).
- [67] U. K. Dey and T. S. Ray, Constraining minimal and non-minimal universal extra dimension models with Higgs couplings, *Phys. Rev. D* **88**, 056016 (2013).
- [68] K. Ghosh, D. Karabacak, and S. Nandi, Constraining bosonic supersymmetry from Higgs results and 8 TeV ATLAS multi-jets plus missing energy data, *J. High Energy Phys.* **09** (2014) 076.
- [69] A. Datta, U. K. Dey, A. Raychaudhuri, and A. Shaw, Boundary localized terms in universal extra-dimensional models through a dark matter perspective, *Phys. Rev. D* **88**, 016011 (2013).
- [70] T. Flacke, D. W. Kang, K. Kong, G. Mohlabeng, and S. C. Park, Electroweak Kaluza-Klein dark matter, *J. High Energy Phys.* **04** (2017) 041.
- [71] A. Datta and A. Shaw, Nonminimal universal extra dimensional model confronts $B_s \rightarrow \mu^+ \mu^-$, *Phys. Rev. D* **93**, 055048 (2016).
- [72] A. Datta and A. Shaw, Effects of non-minimal universal extra dimension on $B \rightarrow X_s \gamma$, *Phys. Rev. D* **95**, 015033 (2017).
- [73] A. Biswas, A. Shaw, and S. K. Patra, $\mathcal{R}(D^{(*)})$ anomalies in light of a nonminimal universal extra dimension, *Phys. Rev. D* **97**, 035019 (2018).
- [74] A. Shaw, Looking for $B \rightarrow X_s \ell^+ \ell^-$ in a nonminimal universal extra dimension model, *Phys. Rev. D* **99**, 115030 (2019).
- [75] T. Jha, Unitarity constraints on non-minimal universal extra dimensional model, *J. Phys. G* **45**, 115002 (2018).
- [76] T. Jha and A. Datta, $Z \rightarrow b\bar{b}$ in non-minimal universal extra dimensional model, *J. High Energy Phys.* **03** (2015) 012.
- [77] T. Jha, Exploration in extra dimension in the era of LHC and beyond, Ph.D. thesis, Calcutta University, 2017.
- [78] S. Dasgupta, U. K. Dey, T. Jha, and T. S. Ray, Status of a flavor-maximal nonminimal universal extra dimension model, *Phys. Rev. D* **98**, 055006 (2018).

- [79] A. Shaw, The impact of nonminimal universal extra dimensional model on $\Delta B = 2$ transitions, *Eur. Phys. J. C* **81**, 137 (2021).
- [80] N. Ganguly and A. Datta, Exploring non minimal universal extra dimensional model at the LHC, *J. High Energy Phys.* **10** (2018) 072.
- [81] U. K. Dey and T. Jha, Rare top decays in minimal and nonminimal universal extra dimension models, *Phys. Rev. D* **94**, 056011 (2016).
- [82] C.-W. Chiang, U. K. Dey, and T. Jha, $t \rightarrow cg$ and $t \rightarrow cZ$ in universal extra-dimensional models, *Eur. Phys. J. Plus* **134**, 210 (2019).
- [83] A. Datta, U. K. Dey, A. Raychaudhuri, and A. Shaw, Universal extra dimensions: Life with BLKs, *J. Phys. Conf. Ser.* **481**, 012006 (2014).
- [84] ATLAS Collaboration, Search for squarks and gluinos in final states with jets and missing transverse momentum using 139 fb^{-1} of $\sqrt{s} = 13 \text{ TeV}$ pp collision data with the ATLAS detector, Technical Report No. ATLAS-CONF-2019-040, CERN, Geneva, 2019.
- [85] M. Cacciari, G. P. Salam, and G. Soyez, The anti- $k(t)$ jet clustering algorithm, *J. High Energy Phys.* **04** (2008) 063.
- [86] M. Cacciari, G. P. Salam, and G. Soyez, FastJet user manual, *Eur. Phys. J. C* **72**, 1896 (2012).
- [87] J. Bjorken and S. J. Brodsky, Statistical model for electron-positron annihilation into hadrons, *Phys. Rev. D* **1**, 1416 (1970).
- [88] J. Alwall, R. Frederix, S. Frixione, V. Hirschi, F. Maltoni, O. Mattelaer, H. S. Shao, T. Stelzer, P. Torrielli, and M. Zaro, The automated computation of tree-level and next-to-leading order differential cross sections, and their matching to parton shower simulations, *J. High Energy Phys.* **07** (2014) 079.
- [89] R. D. Ball *et al.* (NNPDF Collaboration), Parton distributions for the LHC run II, *J. High Energy Phys.* **04** (2015) 040.
- [90] T. Sjostrand, S. Mrenna, and P. Z. Skands, A brief introduction to PYTHIA 8.1, *Comput. Phys. Commun.* **178**, 852 (2008).
- [91] T. Sjostrand, S. Ask, J. R. Christiansen, R. Corke, N. Desai, P. Ilten, S. Mrenna, S. Prestel, C. O. Rasmussen, and P. Z. Skands, An Introduction to PYTHIA 8.2, *Comput. Phys. Commun.* **191**, 159 (2015).
- [92] S. Catani, F. Krauss, B. R. Webber, and R. Kuhn, Qcd matrix elements + parton showers, *J. High Energy Phys.* **01** (2001) 063063.
- [93] J. de Favereau, C. Delaere, P. Demin, A. Giammanco, V. Lemaître, A. Mertens, and M. Selvaggi (DELPHES 3 Collaboration), DELPHES 3, A modular framework for fast simulation of a generic collider experiment, *J. High Energy Phys.* **02** (2014) 057.
- [94] A. Freitas, K. Kong, and D. Wiegand, Radiative corrections to masses and couplings in universal extra dimensions, *J. High Energy Phys.* **03** (2018) 093.
- [95] D. Hooper and S. Profumo, Dark matter and collider phenomenology of universal extra dimensions, *Phys. Rep.* **453**, 29 (2007).
- [96] A. Datta and S. Raychaudhuri, Vacuum stability constraints and LHC searches for a model with a universal extra dimension, *Phys. Rev. D* **87**, 035018 (2013).
- [97] P. Nath and M. Yamaguchi, Effects of Kaluza-Klein excitations on $(g(\mu)-2)$, *Phys. Rev. D* **60**, 116006 (1999).
- [98] K. Agashe, N. Deshpande, and G. Wu, Can extra dimensions accessible to the SM explain the recent measurement of anomalous magnetic moment of the muon?, *Phys. Lett. B* **511**, 85 (2001).
- [99] D. Chakraverty, K. Huitu, and A. Kundu, Effects of universal extra dimensions on B_0 —anti B_0 mixing, *Phys. Lett. B* **558**, 173 (2003).
- [100] A. J. Buras, A. Poschenrieder, M. Spranger, and A. Weiler, The impact of universal extra dimensions on $B \rightarrow X(s)$ gamma, $B \rightarrow X(s)$ gluon, $B \rightarrow X(s)$ mu+ mu-, $K(L) \rightarrow \pi^0 e^+ e^-$ and epsilon-prime/epsilon, *Nucl. Phys.* **B678**, 455 (2004).
- [101] K. Agashe, N. Deshpande, and G. Wu, Universal extra dimensions and $b \rightarrow sy$, *Phys. Lett. B* **514**, 309 (2001).
- [102] J. Oliver, J. Papavassiliou, and A. Santamaria, Universal extra dimensions and $Z \rightarrow b$ anti- b , *Phys. Rev. D* **67**, 056002 (2003).
- [103] T. Appelquist and H.-U. Yee, Universal extra dimensions and the Higgs boson mass, *Phys. Rev. D* **67**, 055002 (2003).
- [104] U. Haisch and A. Weiler, Bound on minimal universal extra dimensions from anti- $B \rightarrow X(s)$ gamma, *Phys. Rev. D* **76**, 034014 (2007).
- [105] T. G. Rizzo and J. D. Wells, Electroweak precision measurements and collider probes of the standard model with large extra dimensions, *Phys. Rev. D* **61**, 016007 (1999).
- [106] A. Strumia, Bounds on Kaluza-Klein excitations of the SM vector bosons from electroweak tests, *Phys. Lett. B* **466**, 107 (1999).
- [107] C. D. Carone, Electroweak constraints on extended models with extra dimensions, *Phys. Rev. D* **61**, 015008 (1999).
- [108] I. Gogoladze and C. Macesanu, Precision electroweak constraints on universal extra dimensions revisited, *Phys. Rev. D* **74**, 093012 (2006).
- [109] P. Dey and G. Bhattacharyya, A comparison of ultraviolet sensitivities in universal, nonuniversal, and split extra dimensional models, *Phys. Rev. D* **70**, 116012 (2004).
- [110] P. Dey and G. Bhattacharyya, Ultraviolet sensitivity of rare decays in nonuniversal extra- dimensional models, *Phys. Rev. D* **69**, 076009 (2004).
- [111] G. Aad *et al.* (ATLAS Collaboration), Search for new phenomena in final states with an energetic jet and large missing transverse momentum in pp collisions at $\sqrt{s} = 8 \text{ TeV}$ with the ATLAS detector, *Eur. Phys. J. C* **75**, 299 (2015); **75**, 408 (2015).
- [112] M. Aaboud *et al.* (ATLAS Collaboration), Search for dark matter and other new phenomena in events with an energetic jet and large missing transverse momentum using the ATLAS detector, *J. High Energy Phys.* **01** (2018) 126.
- [113] T. Flacke, K. Kong, and S. C. Park, A review on non-minimal universal extra dimensions, *Mod. Phys. Lett. A* **30**, 1530003 (2015).
- [114] A. Alloul, N. D. Christensen, C. Degrande, C. Duhr, and B. Fuks, FeynRules 2.0—A complete toolbox for tree-level phenomenology, *Comput. Phys. Commun.* **185**, 2250 (2014).